Explosive multifragmentation in the $^{32}S+^{27}Al$ reaction at 37.5 MeV/nucleon

D. Heuer, A. Chabane, M. E. Brandan,* M. Charvet, A. J. Cole, P. Désesquelles, A. Giorni, A. Lleres, A. Menchaca-Rocha,* and J. B. Viano
Institut des Sciences Nucléaires,
Institut National de Physique Nucléaire et de Physique des Particules–Centre National de la Recherche Scientifique et Université Joseph Fourier, 53 Avenue des Martyrs, F-38026 Grenoble Cedex, France

D. Benchekroun, B. Cheynis, A. Demeyer, E. Gerlic, D. Guinet, M. Stern, and L. Vagneron
Institut de Physique Nucléaire,
Institut National de Physique Nucléaire et de Physique des Particules–Centre National de la Recherche Scientifique et Université Claude Bernard, 43 Boulevard du 11 Novembre 1918, F-69622, Villeurbanne Cedex, France
(Received 22 February 1994)

We describe an experimental study of the $^{32}S+^{27}Al$ reaction at 37.5 MeV/nucleon carried out with the AMPHORA multidetector. A small fraction of events in which the total charge was detected and which are shown to originate mainly from central collisions have been isolated and compared with statistical decay model predictions. Dynamical properties provide strong evidence for a radial directed collective component (blast wave) in the fragment energies which dominates the interfragment Coulomb repulsion and the thermal motion.

PACS number(s): 25.70.Pq, 25.70.Mn

I. INTRODUCTION

The current literature relating to heavy ion collisions at intermediate energies and to the decay of highly excited nuclei contains several experimental studies the results of which seem incompatible [1–5] with the well-known sequential (evaporative) decay mode which successfully describes compound nucleus decay at excitation energies below about 2 MeV/nucleon. Indeed, one branch of current research is devoted to discovering new methods which may be applied to experimental data to provide information concerning the decay mechanism [6–8].

The most popular (easily handled) theories which are based on the assumption that the parent nucleus, prior to decay, may be considered to be in thermal equilibrium also predict that the familiar low-energy evaporative process [9] is progressively replaced at higher excitation energies by a simultaneous dissociation of the parent nucleus into a number of excited prefragments [10–12] which decay into the final "cold" observed nuclei. This multifragmentation decay mode is greatly facilitated by the compressional (and decompressional) effect [13] thought to occur in central collisions. In this case microscopic calculations indicate that the decay takes place from an expanded parent nucleus and that, despite the dynamical aspect of the decompression, may be treated as a statistical process involving all (equally probable) phase space configurations compatible with the "freeze out" volume of the expanded parent (see Ref. [11]). One point of particular interest in these theories is the possible occurence of a phase change which corresponds to the opening up of the multifragment channels.

Coming back to experiment, it is clear that studies of the decay of highly excited nuclei have greatly benefited from the construction and operation of large solid angle multidetectors. Despite limitations mainly due to incomplete solid angle coverage and detector energy thresholds [14] it turns out to be possible, by careful choice of the projectile-target combination, to observe events which are complete in the sense that a significant fraction (in some cases 100%) of the total charge of the entrance channel is detected as products of the reaction. Depending on the reaction (mass asymmetry, energy) it is then possible to attempt, even by event, either the reconstruction of the primary projectilelike fragments (PPLF) in peripheral collisions and deep inelastic reactions, or indeed of the composite nucleus produced in central collisions. In both cases the reconstruction requires some corrective model treatment for undetected neutrons.

We have presented and discussed data for deep inelastic collisions in the 35 MeV/nucleon $^{40}Ca+^{nat}Cu$ system in previous publications [15,16]. In this work we present results on central collisions for the $^{32}S+^{27}Al$ system at 37.5 MeV/nucleon. Once again we concentrate on the analysis of events which are complete in the sense described above. Thus, in the next two sections, we describe the experiment and event selection procedures. The total charge of the projectile-target system is 29. In fact, out of about 3.10^7 events collected in the experiment, about 30 000 events with total detected charge $Z_T = 20$ were observed including a significant fraction containing several intermediate mass fragments ($IMF, Z \geq 3$). The data analysis (Sec. IV) in this work is concentrated on these events. Analysis of global vari-

*Permanent address: IFUNAM, A.P. 20-364, Mexico 01000 DF, Mexico.

ables deduced from the charge partition probabilities and of dynamical quantities shows that our results are incompatible with the binary sequential decay process (we have used the GEMINI code [17]), with a deep inelastic mechanism, and with a simple Coulomb driven prompt dissociation. Indeed, in accordance with certain theoretical predictions [18], our data indicate the presence of a dominant radial collective component (blast wave) in the fragment energies.

II. EXPERIMENTAL PROCEDURE AND DATA REDUCTION

The experiment was carried out using the AMPHORA multidetector with a 37.5 MeV/nucleon ^{32}S beam delivered by the SARA heavy ion accelerator. AMPHORA has been described in detail in previous works [19]. Briefly, it is an azimuthally symmetric detector composed of 140 CsI(Tl) detectors which cover 82% of the full 4π solid angle. The detectors are divided into a forward wall section which contains 48 detectors (2–16°) and a backward ball (16–165°). Thin plastic scintillators (100 and 200 μm) set on forward angle detectors (up to 38°) allow unambiguous identification of charge up to $Z = 9$ and to within ± 1 charge unit for charges less than 20. For those detectors not equipped with scintillator foils identification was limited to charges $Z \leq 3$. For charges 1 and 2 it was possible to make isotopic identification. This phase of data reduction was significantly improved by the creation of semiautomatic masking procedures including automatic detection and correction of gain change [20]. Peripheral collisions were rejected by imposing a multiplicity threshold of 5 in the data acquisition.

Energy calibration was carried out in a separate experiment with the same beam and target as in the main experiment using a silicon tritelescope (50, 150, and 500 μm) backed by a 3 cm CsI(Tl) crystal which measured energy spectra over the full polar angle range covered by the AMPHORA detectors. For each polar angle ring of AMPHORA one detector was selected as a reference, and the gains for other detectors in the same ring adjusted to reproduce the reference detector spectrum. It was then sufficient to calibrate the reference detectors using the energy spectra measured in the calibration run at the corresponding polar angles. For those detectors equipped with plastic scintillators we found (by extending the work of Ref. [21]) that the energy of an ion with charge Z can be written in terms of empirical constants α, β, and γ as

$$E = \{E_s^2 + [\alpha Z L + \beta Z \mathrm{Ln}(1 + \gamma Z^2 L)]^2\}^{1/2} , \qquad (1)$$

where, for each charge Z, E_S is the energy for which the particle stops in the plastic scintillator, and L is the light output of the CsI crystal. We note that the CsI light output is almost proportional to the corresponding energy loss for light ions so that the contribution of the correction (last) term in (1) is small. However, for higher Z the light response becomes noticeably nonlinear. Calibration for charges 1 and 2 was facilitated by the observation of punch through energies in the CsI detectors. The energy thresholds for the CsI crystals were 4 MeV for protons, 7 MeV for alpha particules, and 10 MeV for lithiums. For the plastic foils of 200 μm thickness, they were 4 MeV for protons, 14 MeV for alphas, and 6–10 MeV/nucleon for ions of charges $Z = 5$–15.

For all detectors with a plastic foil, the time of flight was measured using the start signal given by the cyclotron radio frequency. The time separation between two successive bursts was 76 ns. The effective time gate of the data acquisition included four beam bursts in order to estimate chance coincidence event contamination.

III. EVENT SELECTION

Selection of events with total detected charge equal to that of the entrance channel ($Z_T = 29$) provides a strong filter for central collisions. Intuitively, this is obvious due to the fact that targetlike fragments produced in peripheral and midperipheral reactions have insufficient energy to be detected by AMPHORA (due to energy thresholds). In order to make more quantitative estimates of the detection filter effect we have carried out numerical simulations using the code GEMINI [17] to describe decay from an excited composite nucleus produced in central collisions and the code CASCADITA [22] to simulate more peripheral collisions. The detector response was simulated with the filter code SIR [23]. The range of impact parameter associated with central collisions (and thus the range of angular momenta used in the GEMINI simulations) was obtained from a deep inelastic scattering calculation [24] which has been shown in previous work [16] to provide a reasonable description of the impact parameter dependence of energy and angular momentum dissipation. According to this calculation dissipation of all the available entrance channel kinetic energy occurs for impact parameters below 2.5 fm which implies angular momenta up to $45\hbar$. With regard to detection efficiency the main result of the simulations concerns events which contain a single compound nucleus moving with the center of mass velocity (assimilated to central collisions). Selection of the total charge leads to a detection efficiency which is approximately 50 times greater for such events than that observed for events which contain distinct projectilelike and targetlike fragments. Nevertheless, even for events produced from a source moving with the center of mass velocity the absolute efficiency indicated by the simulations is rather small (about 0.5% for events generated by the GEMINI code and 1% for "blast" simulation events to be discussed in Sec. III).

The sample of events selected according to the total detected charge could contain a nonnegligible fraction of random coincidence events. We have used time-of-flight measurements to determine the effect of these coincidences. This procedure is illustrated in Fig. 1. The bold line in Fig. 1(a) represents the distribution of total detected charge, Z_T, for chance coincidence events and is compared with that obtained from the primary event

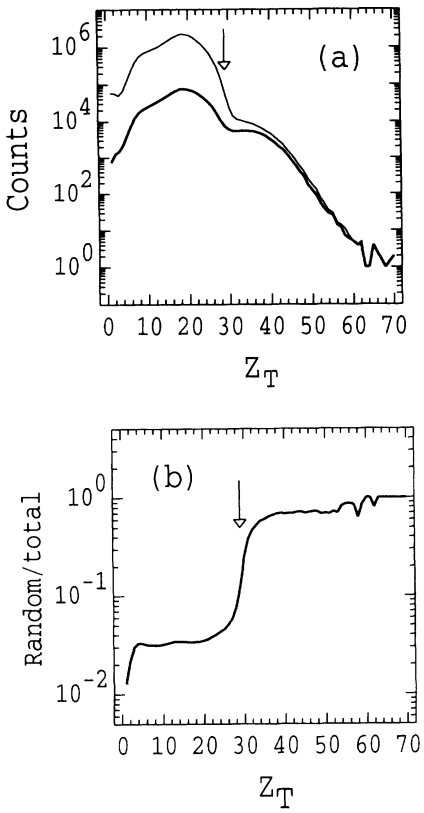

FIG. 1. (a) Distributions of the total detected charge Z_T for all recorded events (thin line) and for chance coincidence events (thick line). (b) Random-to-total ratio as a function of Z_T. The arrows indicate the total charge of the system ($Z_T = 29$).

distribution. The "random-to-total" ratio is shown as a function of Z_T in Fig. 1(b). As the acquisition gate time corresponded to four beam bursts, the probability for chance coincidence events coming from two different bursts is expected to be 75%. Experimentally, from the time-of-flight measurements, we found a value of the random-to-total ratio for $Z_T > 29$ which is in agreement with this estimate [around 70%—see Fig. 1(b)]. The remaining 30% of nonidentified chance coincidences represents 6% of the set of 52 000 "real" events.

An attempt at further selection was made by imposing gates on the total momentum and total energy. Using this method we estimate the nondetected chance coincidence contamination of our selected sample $Z_T = 29$ to be of the order of 3.9%.

An alternative, and more sophisticated technique, is provided by the discriminant analysis method [25]. This technique operates in a vector space each basis vector of which represents a global physical parameter characteristic of a single event (maximum relative velocity between two fragments, total detected charge, total parallel momentum, etc. ... Events are thus represented by points in this space. Two clouds are constructed, one corresponding to random coincidence events identified via their time of flight (see above) and the other to the rest of the events (which include some small residual proportion of random coincidences which are to be eliminated). The random coincidences included in the second group having the same physical features as those in the first one, they should fall in the same region of the vector space. The method consists in finding the axis of projection for which the two clouds are optimally separated. The use of the technique is illustrated in Fig. 2. The bold distribution corresponds to the identified pure chance coincidence cloud. The right-hand bold peak corresponds to chance coincidence events which were not discriminated from the true events by the ten global variables used in our analysis. The figure demonstrates that some chance coincidence events have features so close to real events that, whatever the technique, they cannot be eliminated. The fine traced peak corresponds to real events. A long tail is clearly seen on the left hand side. It corresponds to unidentified random coincidences. These events can thus be eliminated. However, in the remaining event set a small chance coincidence contribution (we estimate about 2%) is impossible to eliminate even using the discriminant method.

The final ($Z_T = 29$) set, in which events containing particles for which the identification was not considered completely satisfactory as well as a small proportion of events with the morphology typical of peripheral collisions were removed, contained 32 000 events. Our simulations indicate that they correspond to an *observed* cross section of about 1.8 mb and thus to a real cross section of approximately 150–200 mb. We have carried out calculations using the BNV code of Bonasera *et al.* [26] which agree with this result in that they predict fusion below 2.5 fm (20 mb).

For this subset we have constructed the spectrum of total energy. This quantity requires estimation of the nonidentified mass corresponding to each detected charge as well as estimation of undetected neutrons. The total energy is then

$$E_{\text{tot}} = E_{\text{kin}} - Q, \tag{2}$$

where E_{kin} and Q are, respectively, the sum of the laboratory kinetic energies of all particles (including undetected neutrons) and the Q value corresponding to the measured charge partition. The masses used to calculate

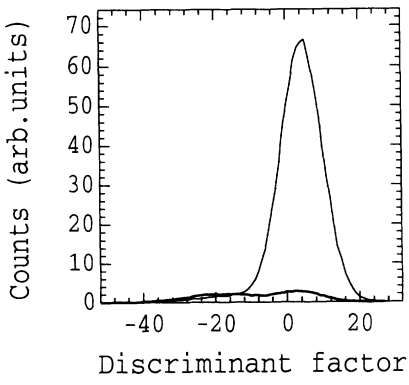

FIG. 2. Distributions of all events (thin line) and random coincidence events (thick line) along the projection axis given by the discriminant analysis method.

the Q values were taken to be those of the most stable isotopes. We have supposed the number of emitted neutrons to be equal to the missing mass (mass of the projectile-target system minus the sum of the estimated masses of the detected reaction products). The neutron kinetic energy was estimated to be the average value of the measured proton kinetic energies with the Coulomb barrier removed. We show, in Fig. 3, the spectrum of the reconstructed total energy $E_{\rm tot}$. The position of the centroid is close to the entrance channel energy (1200 MeV). Thus we can conclude that there are no major systematic errors either in energy calibration or in identification of the charge or in mass estimation used in the reconstruction. This observation is confirmed by the reconstruction of the total energy using "data" from the GEMINI simulation which was filtered by the SIR code prior to the reconstruction procedure. After this filtering procedure the masses of the original fragments were considered unknown. The total energy, which was reconstructed exactly as described above, is again close to 1200 MeV, and the width obtained from the simulation is similar to that obtained from the experimental data (thick trace in Fig. 3).

Finally, we have verified that our reconstruction procedure reproduces the velocity of the center of mass. The expected value is 4.62 cm/ns which should be compared with the experimental value, 4.8±0.4 cm/ns, obtained from the reconstruction procedure. For the GEMINI simulation we obtained a similar value (4.7±0.2 cm/ns).

IV. DATA ANALYSIS

The data discussed in this section includes both static variables (constructed from the measured charge partitions) and dynamic variables. In construction of spectra from model simulations we have systematically taken into account the effect of the detector response and the requirement of total charge detection whenever possible. Thus any distortion of the data due to the detector efficiency is also included in the predictions. It is to be expected that the simulation of such effects, which depend mainly on kinematic properties of the events, is accurate except perhaps in cases where predictions strongly disagree with the data.

One aspect of the data will not be discussed. This concerns center of mass polar angular distributions which are somewhat anisotropic (ratio of counts between 10 and 90 degrees=2). The explanation for this observation may be rather complex. It does not seem to be consistent with a simple angular momentum focusing effect (the angular momenta required to produce the observed asymmetry are typically characteristic of peripheral collisions). It also is not consistent with deep inelastic collisions producing projectilelike and targetlike evaporative sources with velocities close to the center of mass velocity (collisions producing PLF and TLF with a large velocity separation are rejected by the total detected charge constraint). This is due to the fact that the observed anisotropies are identical for both heavy and light fragments whereas they would be expected to diminish with mass (charge) for two finely separated sources (CASCADITA simulations confirm this expectation and produce anisotropies which are too strong). The observed anisotropy may possibly be associated with an intrinsic nonsphericity of the source as suggested by the FOPI group [27]. However, in the present work, we have preferred to treat only the angle integrated distributions and to leave the detailed investigation of the angular dependence for a future publication.

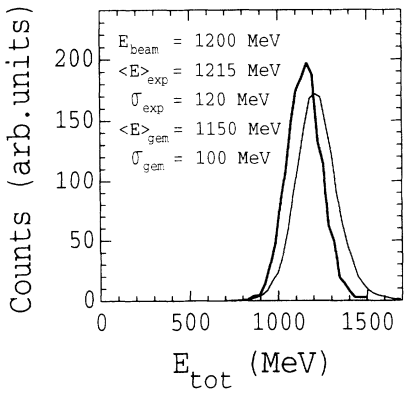

FIG. 3. Experimental spectrum of total energy (thin line) reconstructed for the $Z_T = 29$ events. Also shown (thick line) is the result obtained using events generated by the GEMINI code as described in the text.

A. Comparison of global variables with a percolation simulation

We first discuss certain (static) global variables derived from the observed charge partitions of our sample of $Z_T = 29$ events. We have emphasized, in previous work [15], the strong similarity which exists between these variables and those obtained from percolation simulations made using the simple "bond percolation" process on a cubic lattice. The spectrum of the number of broken bonds was determined by requiring a reproduction of the experimental multiplicity distribution using an automatic iterative technique developed in Ref. [15]. In Figs. 4–6 we show the experimental multiplicity distribution itself (Fig. 4) as well as the inclusive charge distribution (Fig. 5), and the spectrum of the charge of the largest fragment (Fig. 6). By fitting the multiplicity distribution we obtain a satisfactory reproduction of the experimental data in the two latter cases. One can also choose to determine the spectrum of the number of broken bonds by reproduction of the charge distribution or of the distribution of the charge of the heaviest fragment (rather than the multiplicity distribution). In both cases we again succeed in reproducing the global features of the data. This indicates the overall consistency of the percolation simulation with the experimental data. In Fig. 7 we show the spectra of the number of broken bonds obtained from the fits. In all three cases the average value corresponds to a fraction of broken bonds close to 0.7 (the cubic lattice of 29 sites which was considered

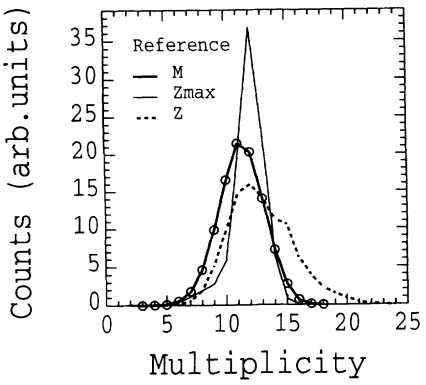

FIG. 4. Experimental multiplicity distribution (circles) compared with percolation calculations (lines). The different curves correspond to the results given by the different reference spectra (multiplicity, largest charge, and inclusive charge) used to obtain the distribution of broken bonds of the percolation simulation.

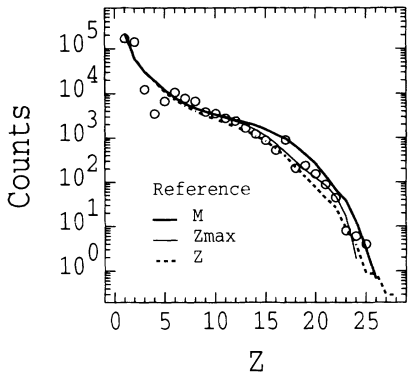

FIG. 5. Experimental inclusive charge distribution (circles) compared to the percolation predictions (lines). Explanation of the different curves as in Fig. 4.

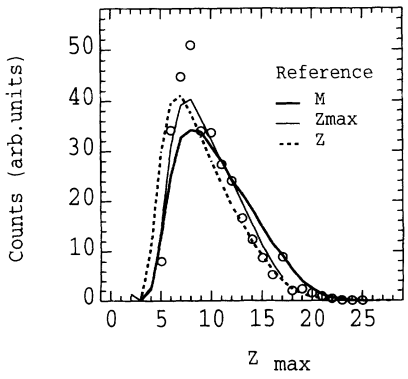

FIG. 6. Experimental distribution of the largest charge (circles) compared with the percolation predictions (lines). Explanation of the different curves as in Fig. 4.

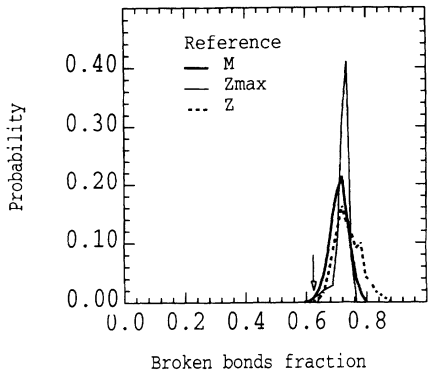

FIG. 7. Distributions of the fraction of broken bonds for the three different percolation fits. The arrow indicates the percolation critical point.

has 64 bonds). The critical point (position of the percolation transition) as determined by examination of the Campi moments [28] is situated at a value of the fraction of broken bonds of 0.625. It thus appears that, in the percolation sense, our data are somewhat "overcritical." Unfortunately, it is not possible to make a more precise statement because of the effect of the detector response (filter) which modifies the observed charge partition weights. This effect is impossible to include in the percolation simulations because of the absence of appropriate dynamics. On the other hand, as we have shown in Ref. [14], the constraint of complete charge detection generally produces multiplicity and charge spectra which are very close to their original "unfiltered" counterparts.

B. Comparison of static and dynamic variables with a binary sequential simulation

We begin with a comparison of the measured inclusive charge distribution with the results of the GEMINI binary sequential decay code. For a simple fusion mechanism with formation of a compound nucleus the excitation energy is 560 MeV (about 10 MeV/nucleon). This situation is, of course, not realized in practice due to the emission of preequilibrium particles which changes not only the identity, but also the excitation energy of the parent nucleus. We have tried to take some account of this mechanism by using the BLANN code [29] to predict the strength of the preequilibrium emission. The effect is important since the code predicts the emission, on average, of 6 preequilibrium protons and a similar number of neutrons (emission of preequilibrium complex particles is not considered). The energies of these particles are calculated by supposing that they are emitted with a characteristic (pseudo) temperature (12 MeV) in the nucleon-nucleon center-of-mass system [30]. With this prescription we find that, on average, more than half of the available center of mass energy is removed by preequilibrium nucleons (the average residual excitation energy is approximately 4 MeV/nucleon).

The charge distribution predicted by the GEMINI code (including preequilibrium nucleon emission, filtering by

the detector response code SIR and selection of total charge) shows significant discrepancies when compared with the data (Fig. 8). This finding is in sharp contrast with the work of Ref. [16] where an excellent description of charge and multiplicity distributions from the decay of excited calciumlike nuclei is obtained (up to 6–7 MeV/nucleon) with the same code. In Fig. 8 the preequilibrium emission of protons calculated as described above has been included in the charge distribution.

In order to test the effect of the preequilibrium contribution on the charge distribution, we have repeated the calculations, suppressing the preequilibrium contribution. The calculated charge distribution is sensitive to this change especially for the higher charges. However, the prediction still significantly underestimates the yields for charges $4 \leq Z \leq 10$. We have also tried varying the preequilibrium pseudo temperature but have been unable to make a significant improvement in the quality of the prediction.

Given the sensitivity of the prediction to the characteristics of the preequilibrium emission we are forced to be rather cautious. For example, we have been unable (with the BLANN code) to explore the effects of preequilibrium emission of alpha particles and heavier charges. Thus we conclude that, while we do observe significant differences between our data and the predictions of the GEMINI code, we cannot, on this basis alone, definitively reject the binary sequential mechanism.

The charge distribution was also generated using the deep inelastic CASCADITA code although this process involved artificially increasing the deep inelastic cross section for small exit channel relative velocities (achieved by diminishing the nucleon mean free path from 5 to 1.5 fm) in order to obtain an *observed* cross section compatible with the experiment [large relative velocities are of course rejected by the requirement of total charge detection (Sec. III)]. However, the predicted charge distribution extends only up to $Z = 14$ (Fig. 8) and thus does not agree with the measurement.

A much more dramatic disagreement with the binary sequential process is observed in the spectrum of the square of the momentum of the largest fragment (P_R^2).

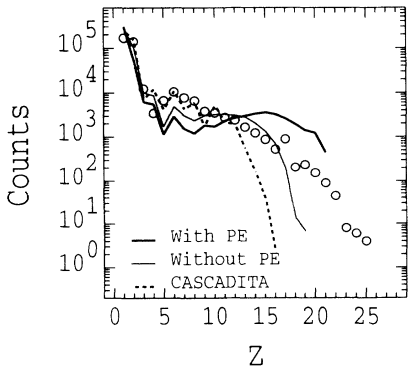

FIG. 8. Comparison of the experimental inclusive charge distribution (circles) with the GEMINI code predictions with and without preequilibrium emission. The deep inelastic CASCADITA prediction is also shown (dotted line).

As pointed out in a previous publication [8], this variable is rather sensitive to the decay mode. In fact, in the case where the largest fragment is a residue resulting from the emission of smaller fragments from the excited parent, the random character of the successive recoil "kicks" results in small values of P_R^2. As shown in Fig. 9 the spectrum predicted by the GEMINI simulations is in total disagreement with the corresponding data.

On the other hand the CASCADITA simulation does, in this case, provide a good description of the data due to the fact that large values of the P_R^2 are generated by the velocity separation of projectilelike and targetlike fragments. Thus, consideration of the P_R^2 variable, while eliminating the sequential binary decay mechanism, is not inconsistent with a deep inelastic process.

A useful way of verifying the importance of this latter mechanism is to be found in the investigation of velocity correlations for events containing three IMF (fragments of charge $Z \geq 3$). Following Ref. [31] the experimental correlation curves were constructed, as a function of the reduced relative velocity (defined in Ref. [4]):

$$V_{\text{red}} = V_{\text{rel}}/\sqrt{Z_1 + Z_2}, \tag{3}$$

where V_{rel} is the relative velocity of the two correlated ions and Z_1, Z_2 their charges. The experimental correlation function (see Fig. 10) rises smoothly and is almost constant for large values of the relative reduced velocity. On the other hand for a double source (deep inelastic reaction) one clearly expects two peaks associated, respectively, with the Coulomb barrier between two fragments from one source and the velocity separation of the two sources. This is confirmed by the CASCADITA simulation which thus exhibits a qualitative disagreement with experiment.

The measured velocity correlation is also quite different from the binary sequential simulation which, with a similar event selection, shows a "Coulomb" peak corresponding to a relative velocity of about 2 cm/ns ($V_{\text{red}}/c \approx 0.020$). We conclude, once again, that our data are in-

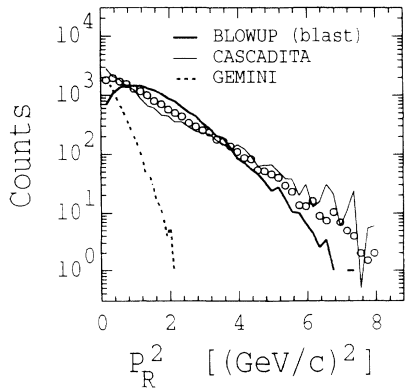

FIG. 9. Experimental spectrum of the square of the momentum of the largest fragment (circles). Comparison with GEMINI, CASCADITA, and the prompt multifragmentation code BLOWUP including Coulomb+thermal ($T = 8.8$ MeV)+blast ($\langle E_{\text{radial}} \rangle = 3.5$ MeV/nucleon) motions.

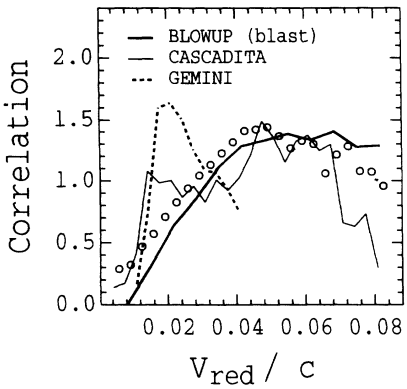

FIG. 10. Same as Fig. 9 but for the correlation function of the reduced relative velocity (see text) between IMF ($Z \geq 3$) for events with exactly three IMF.

compatible with the usual binary sequential decay process. We have checked that these conclusions are not influenced by the presence (or absence) of preequilibrium emission.

C. Comparison with a blast wave simulation

Given the failure of the binary sequential model and the deep inelastic mechanism to account simultaneously for the dynamical variables cited above we have constructed a new simulation code, "BLOWUP" (partly derived from the RIBUST code [7]), which may be used to study dynamical variables in prompt multifragmentation. This code allows the user to place fragments randomly in an initial spherical enclosure (freeze-out volume) and to integrate the corresponding differential equations out to large times. Fragment interactions, angular momentum, radial motion, and thermal (random) motion may all be readily included in the calculations. Events with initial conditions which lead to collision (overlap) of any two fragments during the integration are discarded. The BLOWUP calculations are made event by event by using the experimental charge partitions.

The results of these simulations are rather interesting. They will be discussed in terms of the P_R^2 variable and the velocity correlations discussed in the previous section. The first conclusion is that our results are not compatible with a Coulomb dominated explosion. Indeed, the energy associated with Coulomb repulsion is much too small even for rather compact initial configurations. We have thus made simulations in which the effect of the Coulomb force was supplemented by the introduction of a dominant thermal (Maxwellian distributed) energy component. A reasonable description of the data is obtained only for unrealistically high temperatures (about 44 MeV) which seem incompatible with the estimated excitation energy (in the range 4–10 MeV/nucleon depending on the preequilibrium contribution).

Faced with these inconsistencies, we have been led to introduce a blast wave into the calculation by doting fragments with an initial radially directed energy which is fixed for each fragment by requiring that the fragment velocity is proportional to its distance from the center of mass. The radial energy of all fragments is thus specified by the single value of the velocity at the freeze-out radius (v_f). In the present version of the model the radial momentum is isotropically distributed in the center of mass and, in this sense, is not consistent with the observed angular anisotropy (see above).

The fitting procedure was initially based on the mean value and the variance characterizing the P_R^2 spectrum. However, on the basis of the reproduction of the P_R^2 spectrum alone, we were unable to estimate the contribution of the thermal component. We have thus attempted to optimize the contribution of the thermal component by requiring a satisfactory reproduction of the total energy in the center of mass system. The experimental values used for the fit are thus the mean value $\langle P_R^2 \rangle$, the standard deviation (width) $\sigma(P_R^2)$ and the total center-of-mass energy $E_{\text{c.m.}}$ For a given freeze-out volume the optimum values of the peripheral blast velocity corresponding to each of these three quantities are respectively, v_m, v_s, and v_e. The best fit is obtained, as a function of temperature, by minimizing the dispersion around the average value $(v_m + v_s + v_e)/3$.

Using this criterion the best description of our data (see Fig. 9) is obtained with a blast wave corresponding to an average radially directed energy of 3.5 MeV/nucleon ($v_f = 4.2$ cm/ns) superimposed on a thermal component characterized by a temperature $T = 8.8$ MeV in a freeze out volume corresponding to a density $\rho = 0.03\rho_0$ (ρ_0 is the "normal" nuclear density, taken as 0.17 fm$^-3$). This last quantity is not well determined by the fit except that high densities are not favored. Reconstruction of the measured velocity correlations with these parameters is shown in Fig. 10. The form of the correlation function is quite well reproduced by the calculation over the full range of relative velocities.

It is important to remark that these calculations were made with no specific allowance for preequilibrium emission. The spectra discussed, however, are constructed mainly from the heavier particles and therefore are not directly influenced by the presence of light preequilibrium particles. Of course the neglect of preequilibrium emission can change the velocity of the center of mass system and thus, indirectly, the calculated energies (velocities) of even the heaviest particles. However, a simple calculation shows that, given the symmetry of the system, preequilibrium emission is expected to produce only slight changes in the velocity of the center-of-mass system. For the velocity correlations the question does not arise because only relative velocities are considered.

A final remark has to do with the relative efficiency of AMPHORA for detecting blast events as opposed to binary sequential or deep inelastic events. For the latter we have already explained that the efficiency, estimated using CASCADITA, is incompatible with the experimentally observed count rate. We further find that, globally, binary sequential events are more difficult to detect (by a factor of 2) than blast events. However, any significant contribution from this mechanism should certainly be visible both in the P_R^2 spectrum and in the velocity correlation.

V. SUMMARY AND CONCLUSIONS

The main object of the present work was to present new data obtained with the AMPHORA multidetector in the $^{32}S+^{27}Al$ reaction at 37.5 MeV/nucleon. We have tried to explain the data reduction and selection procedures in some detail.

The analysis was concentrated on events for which the total charge $Z_T = 29$ was observed. Simulation of the detector response indicates that this selection criterion, together with an experimental multiplicity threshold of 5, strongly suppresses deep inelastic collisions.

Quantities obtained from the measured charge partition weights (multiplicity, charge, and largest charge spectra) have been compared with simulations using a simple bond percolation simulation. We find that the data is consistent with a percolation simulation in which the spectrum of broken bonds is characterized by an average value which is above the percolation critical point.

Comparison of our data with statistical model simulations reveals several remarkable and, indeed exciting features. We have found that the measured inclusive charge spectrum exhibits significant discrepancies when compared with the results of a simple sequential decay model even when allowance for preequilibrium emission is made. Moreover, even more striking discrepancies are observed when dynamical variables are included in the analysis. The disagreement between the experimental P_R^2 spectrum with the model prediction is particularly striking. It seems safe to say that our results are in strong disagreement with the binary sequential decay process.

In the course of our investigation we have also been led to consider possible contributions from deep inelastic collisions. We have shown that such contributions cannot be isolated by analysis of the P_R^2 spectrum. However, the absence of a Coulomb peak in the measured velocity correlation for events with three IMF seems to rule out a strong contribution from this mechanism which, in further disagreement with experiment, produces a cut off in the distribution of fragment charge.

We have finally shown that, as far as the (angle integrated) dynamical variables investigated in this work are concerned, it is possible to reproduce the main features observed in the data by the reconstruction of a nuclear blast scenario in which the radial motion of the blast, which corresponds to 3.5 MeV/nucleon, is combined with a random thermal motion and with the interfragment Coulomb repulsion. Fitting the data using only thermal motion associated with Coulomb repulsion leads to unrealistically high temperatures and a strong overestimation of the total fragment kinetic energy.

We feel that, while our results are of considerable qualitative significance, we are only at the beginning of the detailed quantitative investigation of the data. Several paths indicated by recent progress in microscopic theories (e.g., Ref. [26]) need to be explored. Important features of the data (in particular, the anisotropy in the center-of-mass emission pattern) have yet to be examined in detail. A description of these (ongoing) investigations will be left for future publications and is thus beyond the scope of the present work. On the other hand, we should perhaps mention that we have carried out a rather detailed analysis of the probabilities associated with the various charge partitions observed in the experiment. The results of this investigation which, where relevant, are quite consistent with the conclusions of the present study, are presented in a succeeding publication [32].

ACKNOWLEDGMENTS

The authors would like to thank R. J. Charity for providing the code GEMINI. Thanks are also due to R. Bougault, K. Grotowski, R. Planeta, and W. Gawlikowicz for fruitful discussions.

[1] R. Bougault, J. Colin, F. Delauney, A. Genoux-Lubain, A. Hajfani, C. LeBrun, J. F. Lecolley, M. Louvel, and J. C. Steckmeyer, Phys. Lett. B **232**, 291 (1989).

[2] D. H. E. Gross, G. Klotz-Engmann, and H. Oeschler, Phys. Lett. B **224**, 29 (1989).

[3] K. Hagel, M. Gonin, R. Wada, J. B. Natowitz, B. H. Sa, Y. Lou, M. Gui, D. Utley, G. Nebbia, D. Fabris, G. Prete, J. Ruiz, D. Drain, B. Chambon, B. Cheynis, D. Guinet, X. C. Hu, A. Demeyer, C. Pastor, A. Giorni, A. Lleres, P. Stassi, J. B. Viano, and P. Gonthier, Phys. Rev. Lett. **68**, 2141 (1992).

[4] Y. D. Kim *et al.*, Phys. Rev. C **45**, 338 (1992).

[5] D. Fox *et al.*, Phys. Rev. C **47**, R421 (1993).

[6] W. Gawlikowicz and K. Grotowski, Nucl. Phys. **A551**, 73 (1993).

[7] T. Ethvignot, J. M. Alexander, A. J. Cole, A. Elmaani, P. Désesquelles, H. Elhage, A. Giorni, D. Heuer, S. Kox, A. Lleres, F. Merchez, C. Morand, D. Rebreyend, P. Stassi, J. B. Viano, F. Benrachi, B. Chambon, B. Cheynis, D. Drain, and C. Pastor, Phys. Rev. C **48**, 618 (1993).

[8] A. J. Cole, M. E. Brandan, P. Désesquelles, A. Giorni, D. Heuer, A. Lleres, A. Menchaca-Rocha, J. B. Viano, B. Chambon, B. Cheynis, D. Drain, and C. Pastor, Phys. Rev. C **47**, 1251 (1993).

[9] A. J. Cole, N. Longequeue, J. Menet, J. J. Lucas, R. Ost, and J. B. Viano, Nucl. Phys. **A341**, 284 (1980); F. Puhlhofer, *ibid.* **A280**, 267 (1977).

[10] J. A. Lopez and J. Randrup, Nucl. Phys. **A503**, 183 (1989); **A512**, 345 (1990).

[11] D. H. E. Gross, Rep. Prog. Phys. **53**, 605 (1990), and references therein.

[12] J. P. Bondorf, R. Donangelo, I. N. Mishutin, C. J. Pethick, H. Schulz, and K. Sneppen, Nucl. Phys. **A443**, 321 (1987).

[13] S. Leray, C. Ngô, M. E. Spina, B. Rémaud, and F. Sébille, Nucl. Phys. **A511**, 414 (1990); K. Sneppen and L. Vinet, *ibid.* **A480**, 342 (1988); W. Bauer, G. Bertsch, and S. Das Gupta, Phys. Rev. Lett. **58**, 863 (1987).

[14] M. E. Brandan, A. J. Cole, P. Désesquelles, A. Giorni, D. Heuer, A. Lleres, A. Menchaca-Rocha, and K.

Michaelian, Nucl. Instrum. Methods Phys. Res. Sect. A **334**, 461 (1993).
[15] P. Deésesquelles, A. J. Cole, A. Giorni, D. Heuer, A. Lleres, J. B. Viano, B. Chambon, B. Cheynis, D. Drain, and C. Pastor, Phys. Rev. C **48**, 1828 (1993).
[16] A. Lleres, A. Giorni, F. Elhage, M. E. Brandan, A. J. Cole, P. Désesquelles, D. Heuer, A. Menchaca-Rocha, J. B. Viano, F. Benrachi, B. Chambon, B. Cheynis, D. Drain, and C. Pastor, Phys. Rev. C **48**, 2573 (1993).
[17] R. J. Charity, M. A. McMahan, G. J. Wozniak, R. J. McDonald, and L. G. Moretto, Nucl. Phys. **A483**, 371 (1988).
[18] J. P. Bondorf, S. I. A. Garpman, and J. Zimanyi, Nucl. Phys. **A296**, 320 (1978); P. J. Siemens and J. O. Rasmussen, Phys. Rev. Lett. **42**, 880 (1979); P. Danielewicz and Q. Pan, Phys. Rev. C **46**, 2002 (1992).
[19] D. Drain *et al.* Nucl. Instrum. Methods Phys. Res. Sec. A **281**, 528 (1989).
[20] D. Heuer, Nucl. Instrum. Methods Phys. Res. Sect. A **324**, 569 (1993).
[21] D. W. Stracener *et al.*, Nucl. Instrum. Methods Phys. Res. Sect. A **294**, 485 (1990).
[22] A. Menchaca-Rocha, E. Garcia-Solis, and K. Michaelian, Rev. Mexicana Fis. **38**, Suppl. 2, 114 (1992).
[23] Code SIR, D. Heuer *et al.* (unpublished).
[24] J. R. Birkelund, L. E. Tubbs, J. R. Huizenga, J. N. De, and D. Sperber, Phys. Rep. **56**, 107 (1979).
[25] P. Désesquelles, M. Charvet, Report No. ISN 93-53 (unpublished); A. M. Kshirsagar, *Statistics: Textbooks and Monographs Volume 2, Multivariate Analysis* (Marcel Dekker, New York, 1972).
[26] A. Bonasera, F. Gulminelli, and J. M. Molitoris, Phys. Rep. (in press).
[27] S. C. Jeong *et al.*, Phys. Rev. Lett. **72**, 3468 (1994).
[28] X. Campi, J. Phys. A **19**, L917 (1986); J. Phys. (Paris) **48**, C2-151 (1987); Phys. Lett. B **208**, 351 (1991).
[29] M. Blann, Phys. Rev. C **31**, 1245 (1985).
[30] B. Cheynis, B. Chambon, D. Drain, C. Pastor, D. Heuer, A. Dauchy, A. Giorni, C. Morand, and P. Stassi, Z. Phys. A **335**, 77 (1990).
[31] B. Kämpfer *et al.*, Phys. Rev. C **48**, R955 (1993).
[32] A. J. Cole *et al.*, submitted to Phys. Rev. C.